AAS 11-538

CONSTELLATION DESIGN FOR SPACE-BASED SITUATIONAL AWARENESS APPLICATIONS: AN ANALYTICAL APPROACH

Ashley D. Biria* **and Belinda G. Marchand†**

Optimization processes rely on the availability of a pre-defined cost function. Generally, such representations are often analytically available. However, when considering optimal constellation design for space-based space situational awareness applications, a closed-form representation of the cost index is only available under certain assumptions. The present investigation focuses on a subset of cases that admit exact representations. In this case, geometrical arguments are employed to establish an analytical formulation for the coverage area provided as well as for the coverage multiplicity. These analytical results are essential in validating numerical approximations that are able to simulate more complex configurations.

INTRODUCTION

As presently envisioned, space-based space situational awareness (SBSSA) employs a network of space-based sensors to supplement ground sensing capabilities in the detection, tracking, identification, and characterization (DTI&C) of active or passive resident space objects (RSOs). The present investigation focuses specifically on a constellation of space-based sensors, uniformly distributed along a circular orbit. The work is an extension of that previously presented by Marchand and Kobel[1] for a single satellite. Consistent with the assumptions of this earlier study, the present investigation considers only the coverage of a region that exists above the horizon of the satellites and within a pre-specified altitude band. The objective is to maximize the coverage provided by the constellation sensors within the region of interest.

One of the most difficult aspects of this problem is the definition of the cost index, namely the coverage provided by the sensors. As demonstrated by Marchand and Kobel[1] in their initial study, even under extremely simplified assumptions, such as omnidirectional sensors, obtaining a closed-form representation of the cost index is a complex process. Figure 1 illustrates some of the relevant problem parameters in the single satellite case, as defined by Marchand and Kobel.[1]

*Graduate Student, Department of Aerospace Engineering, 210 E. 24th St., Austin, TX 78712. Email: biria@utexas.edu
†Assistant Professor, Department of Aerospace Engineering, 210 E. 24th St., Austin, TX 78712. Email: marchand@alumni.purdue.edu

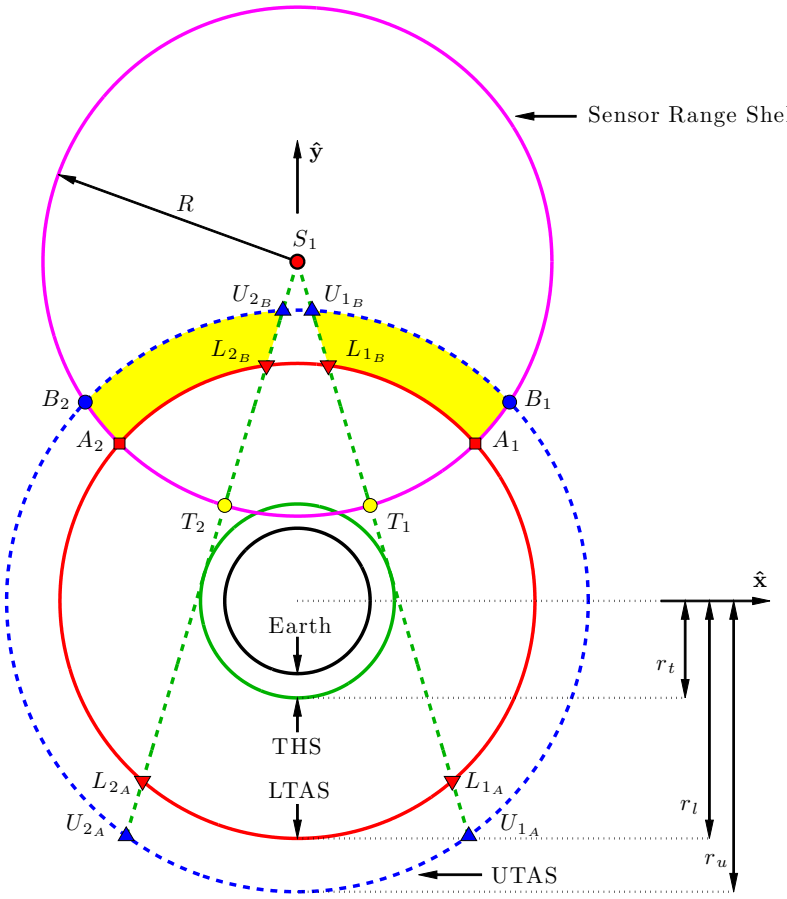

Figure 1. Shell intersections for a single satellite on a circular orbit with coverage area shaded

The three concentric circles in Figure 1 represent reference boundaries; they are the tangent height shell (THS), the lower target altitude shell (LTAS), and the upper target altitude shell (UTAS). The tangent height shell (THS), then, is associated with a user specified reference altitude above the surface of the Earth below which, for instance, atmospheric effects may interfere with sensors. A satellite's horizon is defined as the line originating from the satellite and tangent to the THS. The revolution of the TL in three dimensions traces out a cone, termed here the tangent height cone (THC). The region of interest to the sensors lies outside the THC, within the sensor range shell (RS), and inside the region between the UTAS and LTAS. This region represents a three-dimensional volume, and the constellation's goal is to maximize coverage of this region. Due to the inherent symmetry introduced by the omnidirectional sensor assumption, maximizing the ATH coverage volume is equivalent to maximizing the cross-sectional coverage area.[1] This cross-sectional area of coverage appears shaded in Figure 1. Under these assumptions, a nonlinear piecewise differentiable objective function fully describes the coverage area for all possible satellite altitudes constrained to $r_t \leq r_s < r_{s_3}$, where r_{s_3} is associated with the critical altitude at which no ATH coverage is provided.[1]

This initial work by Marchand and Kobel[1] is a powerful approach for the dual-altitude band problem as compared to previous research on the subject. An older study by Rider[2] also considered

the dual-altitude band ATH problem for constellations in low to medium altitudes with multiple orbital planes, where the satellites lie within or above the dual-altitude band. In his approach, Rider uses spherical geometry and the streets-of-coverage method[3,4] to derive formulas for coverage multiplicity, which is the number of satellites that can simultaneously view a particular region. Rider then relates coverage multiplicity to the required number of orbital planes, required number of satellites per orbital plane, and latitude constraints. Thus, given a desired coverage multiplicity, the required number of sensors for global coverage is completely determined.

The present investigation extends the results of Marchand and Kobel[1] to accommodate multiple satellites with equal omnidirectional sensors uniformly distributed along a circular orbit. An example of such a constellation is depicted in Figure 2. While a similar constellation could be designed

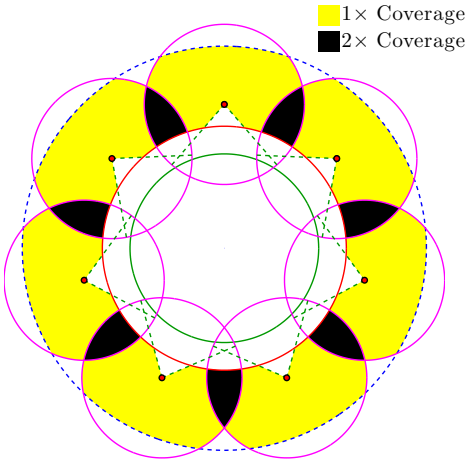

Figure 2. Seven-satellite constellation on a circular orbit

for ATH coverage using Rider's method, the goal here is to establish a foundation for an alternative analytical approach that offers much greater flexibility and the potential to carry that flexibility through to the three-dimensional case. That is to say that in the planar case, using constellation coverage area as a design metric allows for the accommodation of a greater variety of problem specifications and constraints. First, Rider[2] did not consider satellites located between the THS and LTAS. If for some reason the satellite altitude is restricted to be below the LTAS, the coverage area approach offers a solution. Secondly, this coverage area can be used as a cost index in an optimization process that can more clearly describe and lend insight to the quality of a solution.

Of course, there are limitations to this analytical approach. If, for example, more complex sensor profiles are desired, the loss of symmetry makes an analytical solution especially difficult. For such scenarios, a more suitable approach is the numerical method proposed by Takano,[5,6] which uses geometrical arguments similar to those first introduced by Marchand and Kobel[1] but with techniques from computational geometry. Therefore, his method benefits from validation by an analytical approach, which is demonstrated in this investigation as a secondary goal.

To maintain continuity relative to the initial work of Marchand and Kobel,[1] the methodology presented is based on geometrical arguments. First, key shell intersections are determined. Then, based on the spatial interaction of these intersections, geometrical elements are identified for a

unique region of each coverage multiplicity. Finally, a non-unique, nonlinear piecewise differentiable objective function is developed that characterizes the coverage area for $r_t \leq r_s < r_{s_3}$ and maximum coverage multiplicity of $p_{max} = 2$. This restriction is imposed for now because analysis becomes prohibitively complex if greater coverage multiplicities are permitted.

COMPUTING THE TOTAL COVERAGE AREA

The computational methods employed for determining the total coverage area build upon the work of Marchand and Kobel[1] while taking advantage of the inherent symmetry in the constellation. For the single satellite problem, the area computed for S_1 was denoted as $\mathbf{A}$ and referred to a region of 1-fold coverage. For a constellation, an analogous area exists for each satellite i subject to a coverage multiplicity $p \geq 1$, so the notation is modified to $\mathbf{A}_{1\times,i}$ and computed according to the methods described in Marchand and Kobel.[1]

Next, this notation is generalized by first defining $C_{p\times}$ as the collection of regions of coverage multiplicity greater than or equal to p that lie within the "region of interest" — that is, within the dual-altitude band, outside the THC, and within the RS. Similarly, define $C'_{p\times}$ as the collection of regions of coverage multiplicity strictly equal to p that lie within the region of interest. Then, let $\mathbf{A}_{p\times}$ refer to the area of $C_{p\times}$ and $\mathbf{A}'_{p\times}$ refer to the area of $C'_{p\times}$. In fact, $\mathbf{A}_{1\times}$ is the desired total area covered by the entire constellation within the region of interest, but computing it analytically is especially challenging.

As shown by Marchand and Kobel,[1] shell intersections are used to define the vertices of polygons, the areas of which are computed analytically by completely surveying all possible geometries that the intersections of shells could form. For a multi-satellite constellation, even though all shell intersections can be analytically determined with a few equations, the polygon identification process becomes much more cumbersome. Marchand and Kobel[1] showed that it is advantageous to compute the areas of complex geometries by adding up areas of elementary components — triangles, composite triangles, circular sectors and segments — that are easily determined analytically. But for computing coverage area, as the single satellite case requires explicit conditions and equations for each shell configuration, the multi-satellite case requires explicit conditions and equations for each shell configuration and for each coverage multiplicity. This reasoning suggests that $\mathbf{A}_{p_c\times}$, for any coverage multiplicity p_c of interest, could be expressed as a composition of $\mathbf{A}'_{k\times}$ for all $k \in [p_c, p_{max}]$:

$$\mathbf{A}_{p_c\times} \equiv \sum_{k=p_c}^{p_{max}} \mathbf{A}'_{k\times} \tag{1}$$

The quantity $\mathbf{A}_{p_c\times}$ actually has many uses in formulating optimization schemes. Suppose, for example, that it is desired to have continuous 2-fold coverage of the annular region bounded by the dual-altitude band shell, termed AS. In this case, $\mathbf{A}_{2\times}$ should be as close to $\mathbf{A}_{\mathrm{AS}}$ as possible. For the scope of this paper, only the total coverage area is of interest, so Eq. (1) would be used with $p_c = 1$. However, Eq. (1) does not take advantage of the results of Marchand and Kobel,[1] so an alternative approach is presented here that uses $\mathbf{A}_{1\times,i}$.

Consider summing all $\mathbf{A}_{1\times,i}$. By this action, each region $C'_{k\times}$ would be counted k times for all $k \in [2, p_{max}]$. Thus, $\mathbf{A}'_{k\times}$ must be subtracted $k-1$ times from the sum to obtain the actual total coverage area:

$$\mathbf{A}_{1\times} = \sum_{i=1}^{n} \mathbf{A}_{1\times,i} - \sum_{k=2}^{p_{max}} (k-1)\mathbf{A}'_{k\times} \tag{2}$$

Also, observe in Eq. (2) that in general, $\mathbf{A}_{1\times,i}$ could be different for each i, but since the satellites have equal range shells and are uniformly distributed along a circular orbit, the area $\mathbf{A}_{1\times,i}$ is equal for each satellite:

$$\mathbf{A}_{1\times,i} = \mathbf{A}_{1\times,1} \quad \forall\, i \tag{3}$$

Recall that this paper limits the discussion of coverage area calculations to maximum coverage multiplicity $p_{max} = 2$. Let $\mathbf{A}'_{2\times,ij}$ refer to the region formed by the intersection of the range shells of S_i and S_j that is also within the region of interest and subject to strictly 2-fold coverage. Then, $\mathbf{A}'_{2\times}$ is obtained from adding up $\mathbf{A}'_{2\times,ij}$ for all i and j, leading to the following result:

$$\mathbf{A}'_{2\times} \equiv \frac{1}{2}\sum_{i=1}^{n}\sum_{\substack{j=1\\ j\neq i}}^{n}\mathbf{A}'_{2\times,ij} = \sum_{i=1}^{n-1}\sum_{j=i+1}^{n}\mathbf{A}'_{2\times,ij} \tag{4}$$

However, due to the significant symmetry of the problem, strictly 2-fold coverage typically only occurs for pairs of adjacent satellites. As such, this observation is restated as a constraint for further simplicity. Thus, Eq. (4) can be re-expressed as

$$\mathbf{A}'_{2\times} = \mathbf{A}'_{2\times,1n} + \sum_{i=1}^{n-1}\mathbf{A}'_{2\times,i(i+1)} \tag{5}$$

Notice that for $n = 2$ or 3, satellites are adjacent for all possible pairs. As for Eq. (3), since the satellites have equal range shells and are uniformly distributed along a circular orbit, the overlap area $\mathbf{A}'_{2\times,ij}$ is equal for each pair of adjacent satellites. Thus, the derivation arbitrarily focuses on S_1 and S_2 without loss of generality. Furthermore, the number of satellite pairs is equal to the number of satellites, so Eq. (5) becomes

$$\mathbf{A}'_{2\times} = n\mathbf{A}'_{2\times,12} \tag{6}$$

where

$$\mathbf{A}'_{2\times,12} = \begin{cases} \frac{1}{2}\left(\mathbf{A}_{1\times,1} \cap \mathbf{A}_{1\times,2}\right) & n = 2 \\ \mathbf{A}_{1\times,1} \cap \mathbf{A}_{1\times,2} & n > 2 \end{cases} \tag{7}$$

The first case in Eq. (7) is degenerate and differentiated from the second in order for it to function properly with Eq. (2). Finally, by substituting Eq. (6) and Eq. (3) into Eq. (2) and simplifying, Eq. (2) reduces to

$$\mathbf{A}_{1\times} = n\left(\mathbf{A}_{1\times,1} - \mathbf{A}'_{2\times,12}\right) \tag{8}$$

which in conjunction with Eq. (7) is used to compute the total coverage area of the constellation. In fact, much of the following discussion focuses on obtaining analytical formulas for the area defined by Eq. (7).

SHELL INTERSECTIONS

With the extension to satellite constellations, the original 14 key intersections defined by Marchand and Kobel[1] are still valid and defined by the five problem parameters r_s, r_u, r_l, r_t, and R. It is useful to label the original 14 intersections as Type I, defined as those that are associated with only one satellite, occurring between the range shell and a reference boundary or between a tangent line and a reference boundary. However, the analysis is complicated by the manifestation of

new intersection points associated with regions of coverage multiplicity $p > 1$. As is evident from Figure 2, when multiple satellites are introduced, each satellite has associated with it these same 14 intersection points rotated through appropriate multiples of the satellite separation angle,

$$\theta_s = \frac{2\pi}{n} \tag{9}$$

where n, a sixth problem parameter, is the number of satellites in the constellation. In addition to these $14n$ Type I intersections, surfaces associated with one satellite intersecting those of another create new intersections denoted as Type II, which are of a variety that cannot exist in the single satellite case. These changes in geometry necessitate a modified system for labeling intersection points that is illustrated in Figure 3.

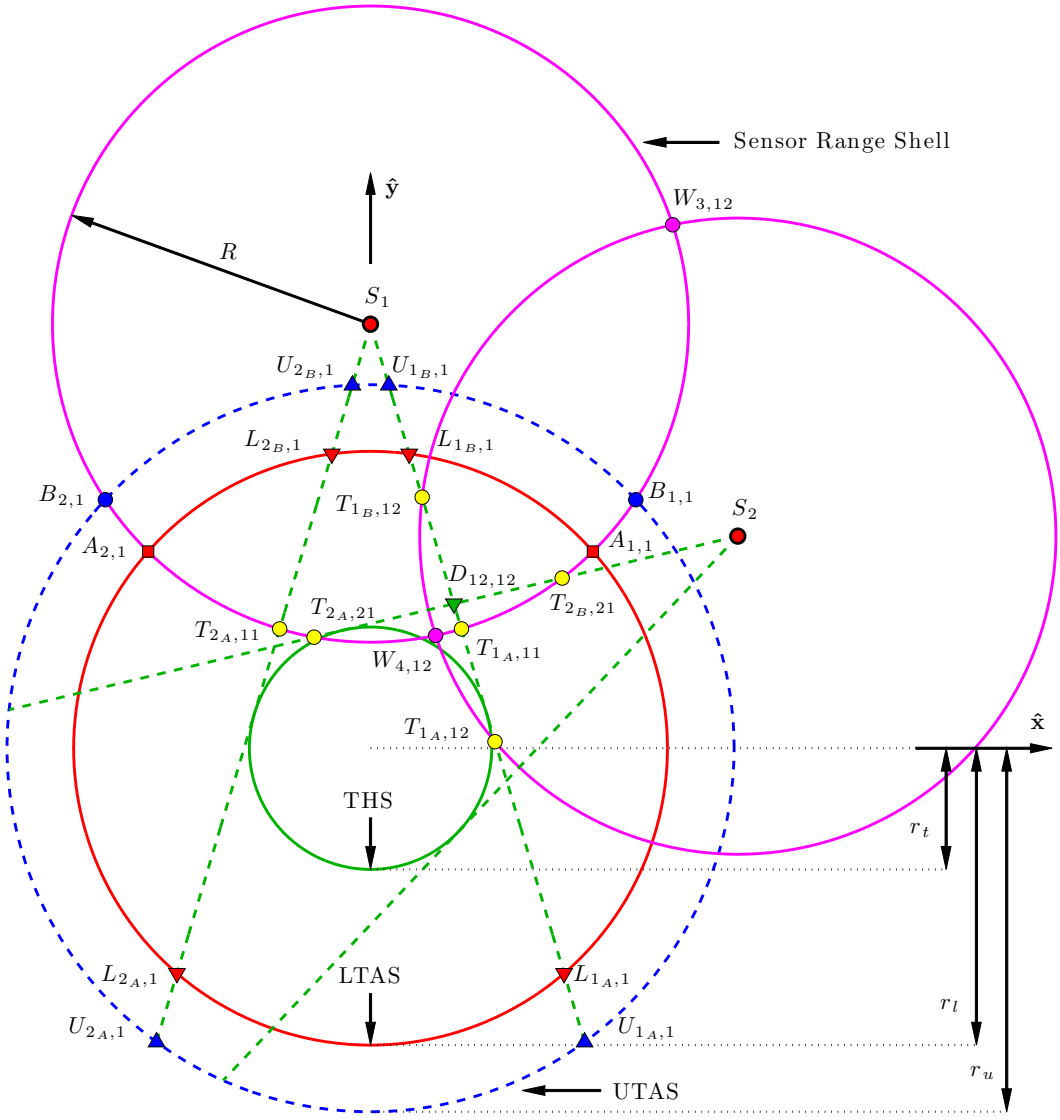

Figure 3. Key shell intersections for a satellite constellation on a circular orbit

The labels for Type I intersections are unchanged with two exceptions. First, a second subscript is appended after a comma to denote the associated satellite. For example, point $B_{2,3}$ refers to point B_2 of S_3. For T intersections, a second and third subscript are appended after a comma. Secondly, points involving the intersection of the TL and RS of one satellite have modified subscripts to accommodate the complexity of Type II intersections. The following are sample transformations from the notation of Marchand and Kobel[1] for Type I intersections of S_1:

$$\begin{aligned} B_2 &\longrightarrow B_{2,1} \\ T_1 &\longrightarrow T_{1_A,11} \end{aligned}$$

Unlike points A, B, L, and U, points T can involve two satellites, thus requiring two numbers after the comma to precisely describe which satellites are associated with that intersection. The first number after the comma refers to the satellite from which the TL originates, and the second number refers to the satellite whose RS intersects that TL. For subscripts *before* the comma, "1" and "2" still indicate intersections to the right and left of a satellite, respectively. To be precise, n rotating coordinate frames $\mathcal{E}_i$, for $i = 1, \ldots, n$, are defined as follows: $\hat{\mathbf{e}}_{2,i}$ is the unit vector directed from the center of the Earth to S_i; $\hat{\mathbf{e}}_{3,i}$ is the unit vector normal to the plane of motion of the satellite constellation, along the angular momentum vector; and $\hat{\mathbf{e}}_{1,i} = \hat{\mathbf{e}}_{2,i} \times \hat{\mathbf{e}}_{3,i}$. In fact, the $\mathcal{E}_1$ frame is identical to the rotating coordinate system used by Marchand and Kobel[1] and all intersections are determined relative to this coordinate system. To facilitate comparison to Marchand and Kobel,[1] a shorthand notation is therefore defined for the $\mathcal{E}_1$ unit vectors: $\hat{\mathbf{x}} = \hat{\mathbf{e}}_{1,1}$, $\hat{\mathbf{y}} = \hat{\mathbf{e}}_{2,1}$, and $\hat{\mathbf{z}} = \hat{\mathbf{e}}_{3,1}$. Thus, for all intersection points, subscript "1" refers to intersections with a positive $\hat{\mathbf{e}}_{1,i}$ component and subscript "2" refers to intersections with a negative $\hat{\mathbf{e}}_{1,i}$ component. The "A" and "B" subscripts have a similar interpretation to that used by Marchand and Kobel,[1] where "A" refers to intersections between a TL of S_i and target shell that are farthest from S_i and "B" refers to intersections between a TL of S_i and target shell that are closest to S_i. Mathematically, these subscripts are used to differentiate the two solutions produced by a quadratic equation, and they are added to the subscript of the T intersections because with the inclusion of Type II intersections, the quadratic equation associated with T intersections can have two valid solutions. For convenience, define the following subscripts for intersections A, B, L, U, T, W, and D:

$$\begin{aligned} &\rho \in \{1, 2\} \\ &\sigma \in \{1_A, 1_B, 2_A, 2_B\} \\ &\tau \in \{3, 4\} \\ &\zeta \in \{1, 2, 1_A, 1_B, 2_A, 2_B\} \equiv \{\rho, \sigma\} \end{aligned} \tag{10}$$

Their use is described throughout the remainder of this section. Should ρ and σ appear in the same equation, then they must be coupled and have the following special relationship:

$$\sigma \in \{\rho_A, \rho_B\} \tag{11}$$

In the single satellite case, the only T intersections are the result of the satellite's TL intersecting its own RS; the TL can only exit the RS because the satellite from which the TL originates is within the RS. However, with Type II intersections in a constellation, a satellite's TL can both enter and exit another's RS. Observe in Figure 3 that if R is increased until S_1 is within the RS of S_2, point $T_{1_B,12}$ disappears while point $T_{1_A,12}$ remains. This is a concrete scenario showing that if only one T intersection truly exists, it must have subscript "A". From this result, a convention for ambiguous

cases is defined. For example, if the intersection of a TL emanating from S_i intersects its own RS, that intersection must be $T_{1_A,ii}$ or $T_{2_A,ii}$.

There are two other intersection points to define: intersections of two range shells and intersections of two tangent lines. The former is indicated with a W and three numbers in the subscript. If the $W_{\tau,ij}$ intersection is farthest from the origin, then $\tau = 3$; if the $W_{\tau,ij}$ intersection is closest to the origin, then $\tau = 4$. The two subscripts after the comma indicate the satellites associated with the intersection, where $i < j$ by convention. The intersection of two tangent lines is marked with $D_{\rho_i\rho_j,ij}$. The ρ_i and ρ_j subscripts are equal to 1 or 2 and respectively indicate which TL of satellite i and j is associated with the intersection. For example, the intersection of the left TL of S_1 with the right TL of S_3 would be denoted as $D_{21,13}$. Again, a convention is imposed such that $i < j$.

As in the single satellite case, the locations of these intersection points are integral to the computation of satellite coverage area. To simplify the determination of intersection points, this approach uses the same rotating coordinate system as implemented by Marchand and Kobel.[1] As depicted in Figure 3, the $\hat{\mathbf{y}}$-axis extends from the Earth to S_1, and the $\hat{\mathbf{x}}$-axis is perpendicular to the $\hat{\mathbf{y}}$-axis and in the plane of the orbit. This rotating coordinate system gives a simple formula for the location of the ith satellite in Cartesian coordinates as

$$(x_{s_i}, y_{s_i}) = (r_s \sin(i-1)\theta_s, r_s \cos(i-1)\theta_s) \tag{12}$$

where the satellites are numbered clockwise in increasing order. Thus, for a constellation with positive angular momentum, S_1 can be viewed as the leading satellite.

Type I Intersections

Let Z be an auxiliary Type I intersection point equal to any of A, B, L, U, or T, which together were used to identify the original 14 intersections published by Marchand and Kobel.[1] Since the original 14 intersections were defined relative to S_1, the correct rotation that gives the remaining $14(n-1)$ Type I intersections is analogous to that used in Eq. (12), which describes the location of each satellite. Thus, all Type I intersections of the constellation can be identified in the $\mathcal{E}_1$ frame as

$$\begin{bmatrix} x_{Z_{\zeta,i}} \\ y_{Z_{\zeta,i}} \end{bmatrix} = \begin{bmatrix} \cos(i-1)\theta_s & \sin(i-1)\theta_s \\ -\sin(i-1)\theta_s & \cos(i-1)\theta_s \end{bmatrix} \begin{bmatrix} x_{Z_{\zeta,1}} \\ y_{Z_{\zeta,1}} \end{bmatrix} \tag{13}$$

which is essentially a clockwise rotation of the input vector. In fact, Eq. (12) is absorbed by Eq. (13) by letting $Z = S$ and disregarding the ζ subscript.

Intersections of Two Range Shells

The intersections of the RS of S_i with the RS of S_j ($W_{3,ij}, W_{4,ij}$) are denoted as $W_{\tau,ij}$, and are most easily computed via the use of coordinate transformations. First, note that the midpoint of a line connecting S_i and S_j is

$$M_{ij} = \left(\frac{x_{s_i} + x_{s_j}}{2}, \frac{y_{s_i} + y_{s_j}}{2} \right) \tag{14}$$

The midpoint is used in the definition of a new reference frame $\mathcal{R}_{ij}$: $\hat{\mathbf{r}}_{2,ij}$ is the unit vector parallel to $\overline{OM_{ij}}$; $\hat{\mathbf{r}}_{3,ij}$ is the unit vector normal to the plane of motion of the satellite constellation, along the angular momentum vector; and $\hat{\mathbf{r}}_{1,ij} = \hat{\mathbf{r}}_{2,ij} \times \hat{\mathbf{r}}_{3,ij}$. The origin of $\mathcal{R}_{ij}$ is chosen to be at M_{ij} because this greatly simplifies the math. For W intersections, S_i has a negative $\hat{\mathbf{r}}_{1,ij}$ component and S_j has a positive $\hat{\mathbf{r}}_{1,ij}$ component by convention. A shorthand for the distance between two

satellites is also defined as $d_{ij} = |\overline{S_i S_j}|$. Interpreting Fewell's[7] result, the general formula for the positive solution of the intersection of two range shells with arbitrary radii is

$$x_{W_{3,ij}} = \frac{R_i^2 - R_j^2 + d_{ij}^2}{2d_{ij}}; \qquad y_{W_{3,ij}} = \frac{1}{2d_{ij}}\sqrt{2d_{ij}^2(R_i^2 + R_j^2) - (R_i^2 - R_j^2)^2 - d_{ij}^4} \tag{15}$$

when viewed in a frame identical to the $\mathcal{R}_{ij}$ frame, but with the origin placed at S_i. Recall that the $\mathcal{R}_{ij}$ frame is defined with equal range shells in mind, so it is known that a line connecting the W intersections must pass through M_{ij}. If the range shells were to have arbitrary radii, then it would be easier to make the coordinates of the $\mathcal{R}_{ij}$ frame identical to those used by Fewell, but this generalization is not presented here. For the purposes of this study, $R_i = R_j$, so Eq. (15) becomes

$$^{\mathcal{R}}x_{W_{3,ij}} = 0; \qquad ^{\mathcal{R}}y_{W_{3,ij}} = \frac{1}{2}\sqrt{4R^2 - d_{ij}^2} \tag{16}$$

where the superscript $\mathcal{R}$ indicates that the coordinates are given in the $\mathcal{R}_{ij}$ frame. It is important to note that Eq. (16) is only valid if $d_{ij} \leq 2R$ so that the coordinates are real numbers. Furthermore, symmetry implies that

$$^{\mathcal{R}}x_{W_{4,ij}} = {}^{\mathcal{R}}x_{W_{3,ij}}; \qquad ^{\mathcal{R}}y_{W_{4,ij}} = -{}^{\mathcal{R}}y_{W_{3,ij}} \tag{17}$$

Transforming these intersections to the $\mathcal{E}_1$ frame requires both a rotation by angle η and a translation, where η is the angle between the $\hat{\mathbf{y}}$ and $\hat{\mathbf{r}}_{2,ij}$ unit vectors. Using a fundamental property of the dot product,

$$\eta = \cos^{-1}\left(\hat{\mathbf{y}} \cdot \hat{\mathbf{r}}_{2,ij}\right) \tag{18}$$

which enforces the condition that $0 \leq \eta \leq \pi$; however, this does not distinguish between clockwise and counterclockwise rotations and is undesirable. Thus, Eq. (18) is corrected by adding the following convention: $\eta > 0$ if $\hat{\mathbf{r}}_{2,ij}$ has a positive $\hat{\mathbf{x}}$ component and $\eta < 0$ if $\hat{\mathbf{r}}_{2,ij}$ has a negative $\hat{\mathbf{x}}$ component, which determines whether the appropriate rotation is clockwise or counterclockwise. Re-expressing Eq. (18) with this correction gives:

$$\eta = \begin{cases} +\cos^{-1}\left(\hat{\mathbf{y}} \cdot \hat{\mathbf{r}}_{2,ij}\right), & \text{if } \hat{\mathbf{x}} \cdot \hat{\mathbf{r}}_{2,ij} > 0 \\ -\cos^{-1}\left(\hat{\mathbf{y}} \cdot \hat{\mathbf{r}}_{2,ij}\right), & \text{if } \hat{\mathbf{x}} \cdot \hat{\mathbf{r}}_{2,ij} < 0 \end{cases} \tag{19}$$

Lastly, the translation, which is associated with the displacement between the origin of each frame, must be properly handled by shifting $x_{M_{ij}}$ in the $\hat{\mathbf{x}}$ direction and $y_{M_{ij}}$ in the $\hat{\mathbf{y}}$ direction. Then, the total transformation from the $\mathcal{R}_{ij}$ frame to the $\mathcal{E}_1$ frame is

$$^{\mathcal{E}_1}\begin{bmatrix} x_{W_{\tau,ij}} \\ y_{W_{\tau,ij}} \end{bmatrix} = \begin{bmatrix} \cos\eta & \sin\eta \\ -\sin\eta & \cos\eta \end{bmatrix} {}^{\mathcal{R}_{ij}}\begin{bmatrix} x_{W_{\tau,ij}} \\ y_{W_{\tau,ij}} \end{bmatrix} + {}^{\mathcal{E}_1}\begin{bmatrix} x_{M_{ij}} \\ y_{M_{ij}} \end{bmatrix} \tag{20}$$

For $\eta > 0$, the direction cosine matrix gives a counterclockwise rotation of the frame. Should $d_{ij} = 2R$, then the two range shells intersect at only one point.

Intersections of Two Tangent Lines

The intersections of a TL of S_i and a TL of S_j are denoted as $D_{\rho_i\rho_j,ij}$ in the most general form. This gives four possible D intersections per satellite pair, collectively identified as ($D_{11,ij}$, $D_{12,ij}$, $D_{21,ij}$, $D_{22,ij}$). For certain geometries, it is possible that less than four intersections exist, such as

when two TLs are parallel or when they diverge. First, some results from Marchand and Kobel[1] must be generalized for constellations. One result states that the TL of S_1 is tangent to the THS when

$$\theta_t = \cos^{-1}\left(\frac{r_t}{r_s}\right) \tag{21}$$

which actually holds for any TL, where θ_t is the above-the-horizon coverage angle at the point of tangency. The slope of each TL of S_i can then be expressed in terms of the satellite location and the points of tangency as follows:

$$m_{\rho,i} = \frac{y_{t_{\rho,i}} - y_{s_i}}{x_{t_{\rho,i}} - x_{s_i}} \tag{22}$$

for

$$\begin{aligned} x_{t_{\rho,i}} &= \begin{cases} r_t \sin\left[(i-1)\theta_s + \theta_t\right] & \text{if } \rho = 1 \\ r_t \sin\left[(i-1)\theta_s - \theta_t\right] & \text{if } \rho = 2 \end{cases} \\ y_{t_{\rho,i}} &= \begin{cases} r_t \cos\left[(i-1)\theta_s + \theta_t\right] & \text{if } \rho = 1 \\ r_t \cos\left[(i-1)\theta_s - \theta_t\right] & \text{if } \rho = 2 \end{cases} \end{aligned} \tag{23}$$

Each intersection is given by the solution to the following system of equations:

$$y_{D_{\rho_i\rho_j,ij}} = m_{\rho_i,i} x_{D_{\rho_i\rho_j,ij}} + b_{\rho_i,i}; \qquad y_{D_{\rho_i\rho_j,ij}} = m_{\rho_j,j} x_{D_{\rho_i\rho_j,ij}} + b_{\rho_j,j} \tag{24}$$

where b is the y-coordinate of the point at which the TL intersects the $\hat{\mathbf{y}}$-axis, determined as

$$b_{\rho_i,i} = y_{s_i} - m_{\rho_i,i} x_{s_i}; \qquad b_{\rho_j,j} = y_{s_j} - m_{\rho_j,j} x_{s_j} \tag{25}$$

Using Eq. (24) to solve for $x_{D_{\rho_i\rho_j,ij}}$ by substitution gives

$$x_{D_{\rho_i\rho_j,ij}} = \frac{b_{\rho_i,i} - b_{\rho_j,j}}{m_{\rho_i,i} - m_{\rho_j,j}} \tag{26}$$

Then, substituting Eq. (25) into Eq. (24) and Eq. (26) gives

$$x_{D_{\rho_i\rho_j,ij}} = \frac{m_{\rho_i,i} x_{s_i} - m_{\rho_j,j} x_{s_j} - y_{s_i} + y_{s_j}}{m_{\rho_i,i} - m_{\rho_j,j}}; \qquad y_{D_{\rho_i\rho_j,ij}} = m_{\rho_i,i}(x_{D_{\rho_i\rho_j,ij}} - x_{s_i}) + y_{s_i} \tag{27}$$

Of course, Eqs. (26) and (27) are not valid if $m_{\rho_i,i} = m_{\rho_j,j}$ since the denominator would go to zero. Such a scenario implies that the intersection does not exist, which makes sense physically because two parallel lines cannot intersect, assuming they are not collinear. Should two TLs happen to be collinear, $D_{\rho_i\rho_j,ij}$ becomes meaningless and adds no new information to the geometry. Further observe that Eq. (27) assumes each TL is a line, though in reality the TL does not extend above the satellite from which it originates. Thus, care should be taken to ignore a solution given by Eq. (27) if the computed intersection is located above the satellites from which each TL emanates.

Type II Intersections of Tangent Lines with Range Shells

The intersection of a TL of S_i with the RS of S_j for $i \neq j$ is a Type II intersection denoted as $T_{\sigma,ij}$. There are at most four such T intersections per satellite pair, collectively identified as ($T_{1_A,ij}$, $T_{1_B,ij}$, $T_{2_A,ij}$, $T_{2_B,ij}$). Note the application of Eq. (11) to Eqs. (28–30). The coordinates are given by the solution to the following system of equations:

$$\left(x_{T_{\sigma,ij}} - x_{s_j}\right)^2 + \left(y_{T_{\sigma,ij}} - y_{s_j}\right)^2 = R^2; \qquad y_{T_{\sigma,ij}} = m_{\rho,i} x_{T_{\sigma,ij}} + b_{\rho,i} \tag{28}$$

where $b_{\rho,i}$ is interpreted as $b_{\rho,i} = y_{s_i} - m_{\rho,i}x_{s_i}$ from Eq. (25). In general, solving Eq. (28) for $x_{T_{\sigma,ij}}$ gives

$$x_{T_{\sigma,ij}} = \frac{-\left[m_{\rho,i}\left(b_{\rho,i} - y_{s_j}\right) - x_{s_j}\right] \pm \sqrt{(m_{\rho,i}^2+1)R^2 - \left(b_{\rho,i} - y_{s_j} + m_{\rho,i}x_{s_j}\right)^2}}{m_{\rho,i}^2 + 1} \tag{29}$$

which has at most two real solutions. It has no real solution if $(m_{\rho,i}^2+1)R^2 < (b_{\rho,i}-y_{s_j}+m_{\rho,i}x_{s_j})^2$. However, Eq. (29) has an issue analogous to that of Eq. (27), which is that if the TL originates within the RS, it will still give two real solutions even if one or no T intersections exist. Should only one T intersection exist, ignore the $T_{\rho_B,ij}$ intersection. If no T intersections exist, then disregard both solutions to Eq. (29); this situation arises when the entire TL is within the RS.

Determining which solution corresponds to subscript "A" and which to subscript "B" is nontrivial and is summarized as

$$x_{T_{\rho_A,ij}} = \begin{cases} x^+_{T_{\sigma,ij}}, & \text{if } x_{s_i} < 0 \\ x^-_{T_{\sigma,ij}}, & \text{if } x_{s_i} = 0, y_{s_i} > 0, m_{\rho,i} > 0 \\ x^+_{T_{\sigma,ij}}, & \text{if } x_{s_i} = 0, y_{s_i} > 0, m_{\rho,i} < 0 \\ x^+_{T_{\sigma,ij}}, & \text{if } x_{s_i} = 0, y_{s_i} < 0, m_{\rho,i} > 0 \\ x^-_{T_{\sigma,ij}}, & \text{if } x_{s_i} = 0, y_{s_i} < 0, m_{\rho,i} < 0 \\ x^-_{T_{\sigma,ij}}, & \text{if } x_{s_i} > 0 \end{cases} \tag{30}$$

where $x^+_{T_{\sigma,ij}}$ corresponds to the solution of Eq. (29) with the positive square root term and $x^-_{T_{\sigma,ij}}$ corresponds to the solution of Eq. (29) with the negative square root term. Then, $x_{T_{\rho_B,ij}}$ is the other solution of Eq. (29) not defined by Eq. (30). The complete solution to the system of equations given in Eq. (28) is then formed by using Eqs. (29–30) in conjunction with the equation for the TL in Eq. (28).

GEOMETRICAL ELEMENTS OF REGIONS SUBJECT TO 2-FOLD COVERAGE

As demonstrated by Marchand and Kobel[1] for the single satellite case, the coverage area is at best reduced to a continuous piecewise differentiable function, and the same holds for areas subject to 2-fold coverage in a constellation. The area of overlap $\mathbf{A}'_{2\times,ij}$ refers to the area of a region $C'_{2\times,ij}$ between two satellites that is within view of both satellites. Recall that for 2-fold coverage restricted to pairs of adjacent satellites, $C'_{2\times,12}$ can be analyzed instead without loss of generality. This region is a polygon whose vertices are connected by lines and/or circular arcs, and which can have 16 unique shapes, categorized according to the number of vertices that the overlap area has. Table 1 shows the relation between the number of vertices and number of unique shapes.

Table 1. Relation between the Number of Vertices and Number of Unique Shapes for $C'_{2\times,12}$

Number of Vertices	Number of Unique Shapes
2	1
3	3
4	3
5	3
6	3
7	2
8	1

Due to the geometry of the problem, $C'_{2\times,12}$ cannot have greater than eight vertices. The following discussion defines all of the fundamental geometrical elements necessary for creating a piecewise differentiable function for the 2-fold coverage area $\mathbf{A}'_{2\times,12}$, using a combination of triangles, quadrilaterals, and circular segments. The area $\mathbf{A}'_{2\times,12}$ is then computed by summing the areas of the appropriate fundamental shapes.

For the 3-vertex cases, new composite triangles must be defined. Case 3.i requires the definition of a new composite triangle, Λ_3, made up of three arcs:

$$\begin{aligned}\mathbf{A}_{\Lambda_3}(r_l,R,|\overline{A_{1,1}A_{2,2}}|,|\overline{A_{1,1}W_{3,12}}|,|\overline{A_{2,2}W_{3,12}}|) = \\ \mathbf{A}_{\triangle}(|\overline{A_{1,1}A_{2,2}}|,|\overline{A_{1,1}W_{3,12}}|,|\overline{A_{2,2}W_{3,12}}|)- \\ \mathbf{A}_{\Sigma}(r_l,|\overline{A_{1,1}A_{2,2}}|)+\mathbf{A}_{\Sigma}(R,|\overline{A_{1,1}W_{3,12}}|)+\mathbf{A}_{\Sigma}(R,|\overline{A_{2,2}W_{3,12}}|)\end{aligned} \tag{31}$$

$\mathbf{A}_{\triangle}$ refers to the area of a triangle computed using Heron's formula, where each argument is a side of the triangle.[1] $\mathbf{A}_{\Sigma}$ refers to the area of a circular segment, where the first argument is the circle's radius and the second is the associated chord.[1] The equation for $\mathbf{A}_{\Lambda_3}$ adds an $\mathbf{A}_{\Sigma}$ term to the definition of $\mathbf{A}_{\Lambda_1}$. For case 3.ii, a new composite triangle, Λ_4, is defined, also made up of three arcs but with different convexity:

$$\begin{aligned}\mathbf{A}_{\Lambda_4}(r_u,R,|\overline{B_{1,1}B_{2,2}}|,|\overline{B_{1,1}W_{4,12}}|,|\overline{B_{2,2}W_{4,12}}|) = \\ \mathbf{A}_{\triangle}(|\overline{B_{1,1}B_{2,2}}|,|\overline{B_{1,1}W_{4,12}}|,|\overline{B_{2,2}W_{4,12}}|)+ \\ \mathbf{A}_{\Sigma}(r_u,|\overline{B_{1,1}B_{2,2}}|)+\mathbf{A}_{\Sigma}(R,|\overline{B_{1,1}W_{4,12}}|)+\mathbf{A}_{\Sigma}(R,|\overline{B_{2,2}W_{4,12}}|)\end{aligned} \tag{32}$$

The equation for $\mathbf{A}_{\Lambda_4}$ is similar to that for $\mathbf{A}_{\Lambda_3}$ except all circular segment areas are added to the base triangle. A new composite triangle, Λ_5, must be defined for case 3.iii.a and 3.iii.b. Λ_5 is pie-shaped, consisting of one arc and two line segments:

$$\begin{aligned}\mathbf{A}_{\Lambda_5}(r_u,|\overline{U_{2_A,2}U_{1_A,1}}|,|\overline{U_{2_A,2}D_{12,12}}|,|\overline{U_{1_A,1}D_{12,12}}|) = \\ \mathbf{A}_{\triangle}(|\overline{U_{2_A,2}U_{1_A,1}}|,|\overline{U_{2_A,2}D_{12,12}}|,|\overline{U_{1_A,1}D_{12,12}}|)+\mathbf{A}_{\Sigma}(r_u,|\overline{U_{2_A,2}U_{1_A,1}}|)\end{aligned} \tag{33}$$

The equation for $\mathbf{A}_{\Lambda_5}$ is similar to that for $\mathbf{A}_{\Lambda_2}$ except that the circular segment area is added to the base triangle.

For overlap areas with greater than three vertices, it is helpful to introduce the concept of a composite quadrilateral and define an additional composite triangle, Λ_6:

$$\begin{aligned}\mathbf{A}_{\Lambda_6}(R,R,|\overline{T_{2_A,21}W_{4,12}}|,|\overline{W_{4,12}T_{1_A,12}}|,|\overline{T_{1_A,12}T_{2_A,21}}|) = \\ \mathbf{A}_{\triangle}(|\overline{T_{2_A,21}W_{4,12}}|,|\overline{W_{4,12}T_{1_A,12}}|,|\overline{T_{1_A,12}T_{2_A,21}}|)+ \\ \mathbf{A}_{\Sigma}(R,|\overline{T_{2_A,21}W_{4,12}}|)+\mathbf{A}_{\Sigma}(R,|\overline{W_{4,12}T_{1_A,12}}|)\end{aligned} \tag{34}$$

Formulas for the areas of composite quadrilaterals are derived from the general formula for the area of a convex quadrilateral based on its diagonals.[8] For a convex quadrilateral $abcd$, define the following diagonals:

$$\begin{aligned}\mathbf{c}_1 &= (x_c - x_a)\hat{\mathbf{x}} + (y_c - y_a)\hat{\mathbf{y}} \\ \mathbf{c}_2 &= (x_d - x_b)\hat{\mathbf{x}} + (y_d - y_b)\hat{\mathbf{y}}\end{aligned} \tag{35}$$

The area of quadrilateral $abcd$ can then be expressed as

$$\mathbf{A}_{\square} = \frac{1}{2}|\mathbf{c}_1 \times \mathbf{c}_2| \tag{36}$$

Six types of composite quadrilaterals are introduced. For case 4.i.a, the area of overlap can be described as a composite quadrilateral $\mathbf{A}_{\Pi_1}$, defined as

$$\begin{aligned}\mathbf{A}_{\Pi_1}(r_u,r_l,U_{1_B,1},U_{2_B,2},L_{2_B,2},L_{1_B,1}) = \mathbf{A}_{\square}(U_{1_B,1},U_{2_B,2},L_{2_B,2},L_{1_B,1})+\\ +\mathbf{A}_{\Sigma}(r_u,|\overline{U_{1_B,1}U_{2_B,2}}|)-\mathbf{A}_{\Sigma}(r_l,|\overline{L_{2_B,2}L_{1_B,1}}|)\end{aligned} \tag{37}$$

The five remaining types of composite quadrilaterals are defined in Eqs. (38–42). They all use a similar construction, in which circular segments are added or subtracted from a base convex quadrilateral.

$$\begin{aligned}\mathbf{A}_{\Pi_2}(r_u,r_l,R,B_{2,2},B_{1,1},A_{1,1},A_{2,2}) = \mathbf{A}_{\square}(B_{2,2},B_{1,1},A_{1,1},A_{2,2})+\\ \mathbf{A}_{\Sigma}(r_u,|\overline{B_{2,2}B_{1,1}}|)-\mathbf{A}_{\Sigma}(r_l,|\overline{A_{1,1}A_{2,2}}|)+\\ \mathbf{A}_{\Sigma}(R,|\overline{B_{1,1}A_{1,1}}|)+\mathbf{A}_{\Sigma}(R,|\overline{A_{2,2}B_{2,2}}|)\end{aligned} \tag{38}$$

$$\begin{aligned}\mathbf{A}_{\Pi_3}(R,R,W_{3,12},T_{2_B,21},D_{12,12},T_{1_B,12}) = \mathbf{A}_{\square}(W_{3,12},T_{2_B,21},D_{12,12},T_{1_B,12})+\\ \mathbf{A}_{\Sigma}(R,|\overline{W_{3,12}T_{2_B,21}}|)+\mathbf{A}_{\Sigma}(R,|\overline{T_{1_B,12}W_{3,12}}|)\end{aligned} \tag{39}$$

$$\begin{aligned}\mathbf{A}_{\Pi_4}(r_u,R,R,B_{2,2},B_{1,1},T_{2_B,21},T_{1_B,12}) = \mathbf{A}_{\square}(B_{2,2},B_{1,1},T_{2_B,21},T_{1_B,12})+\\ \mathbf{A}_{\Sigma}(r_u,|\overline{B_{2,2}B_{1,1}}|)+\mathbf{A}_{\Sigma}(R,|\overline{B_{1,1}T_{2_B,21}}|)+\mathbf{A}_{\Sigma}(R,|\overline{T_{1_B,12}B_{2,2}}|)\end{aligned} \tag{40}$$

$$\begin{aligned}\mathbf{A}_{\Pi_5}(r_u,U_{1_B,1},U_{2_B,2},T_{2_A,21},T_{1_A,12}) = \mathbf{A}_{\square}(U_{1_B,1},U_{2_B,2},T_{2_A,21},T_{1_A,12})+\\ \mathbf{A}_{\Sigma}(r_u,|\overline{U_{1_B,1}U_{2_B,2}}|)\end{aligned} \tag{41}$$

$$\begin{aligned}\mathbf{A}_{\Pi_6}(r_l,R,R,A_{1,1},A_{2,2},T_{1_A,12},T_{2_A,21}) = \mathbf{A}_{\square}(A_{1,1},A_{2,2},T_{1_A,12},T_{2_A,21})-\\ \mathbf{A}_{\Sigma}(r_l,|\overline{A_{1,1},A_{2,2}}|)+\mathbf{A}_{\Sigma}(R,|\overline{A_{2,2},T_{1_A,12}}|)+\mathbf{A}_{\Sigma}(R,|\overline{T_{2_A,21}A_{1,1}}|)\end{aligned} \tag{42}$$

ABOVE-THE-HORIZON 2-FOLD COVERAGE AREA FOR A CONSTELLATION IN A CIRCULAR ORBIT

The 2-fold area computations are organized in a way that emphasizes the relationship expressed in Table 1. Table 2 identifies the conditions that must be satisfied for each of 22 possible cases and outlines the naming convention used. The first number denotes the number of vertices and the second number denotes the type. Thus, shape 3.ii is a 3-vertex overlap area of type II. Cases are labeled with an "a" or "b" when the shape is the same but some of the vertices are different intersection points. This is why there are 22 cases for only 16 unique shapes.

Once the case is identified from Table 2, the appropriate formula for computing the 2-fold coverage area is found in Table 3. As mentioned previously, the way that each complex shape is divided into more fundamental shapes is not unique, and Table 3 merely shows one possible scheme. Effort is also made to describe the geometry in a systematic way. For example, quadrilaterals are labeled clockwise from the top-left corner, and fundamental areas are summed in the order in which they are stacked within the complex shape. Figure 4 contains clear examples of each of the 22 cases, zoomed in on the region $C'_{2\times,12}$.

Table 2. Conditions for Identifying the Overlap Area Polygon $C'_{2\times,12}$

Conditions	Shape Type
$r_l < \lvert\overline{OW_{4,12}}\rvert < \lvert\overline{OM_{12}}\rvert$, $\lvert\overline{OD_{12,12}}\rvert < \lvert\overline{OW_{4,12}}\rvert < \lvert\overline{OM_{12}}\rvert$, $\lvert\overline{OW_{3,12}}\rvert < r_u$, $\lvert\overline{OT_{1_B,12}}\rvert < \lvert\overline{OW_{4,12}}\rvert < \lvert\overline{OM_{12}}\rvert$	2
$\lvert\overline{OD_{12,12}}\rvert < r_l$, $x_{W_{4,12}} < r_l \sin(\theta_s/2)$, $r_l < \lvert\overline{OW_{3,12}}\rvert \leq r_u$, $\lvert\overline{OT_{1_B,12}}\rvert < r_l$	3.i
$r_l < \lvert\overline{OW_{4,12}}\rvert < \lvert\overline{OM_{12}}\rvert$, $\lvert\overline{OD_{12,12}}\rvert < \lvert\overline{OW_{4,12}}\rvert < \lvert\overline{OM_{12}}\rvert$, $r_u < \lvert\overline{OW_{3,12}}\rvert$, $\lvert\overline{D_{12,12}S_1}\rvert < \lvert\overline{T_{1_A,12}S_1}\rvert$, $\lvert\overline{D_{12,12}S_1}\rvert < \lvert\overline{T_{1_B,12}S_1}\rvert$	3.ii
$r_l \leq r_s$, $\lvert\overline{D_{12,12}S_1}\rvert < \lvert\overline{L_{1_B,1}S_1}\rvert$, $x_{W_{4,12}} < x_{D_{12,12}}$, $r_u \leq \lvert\overline{OT_{1_B,12}}\rvert$	3.iii.a
$\lvert\overline{L_{1_A,1}S_1}\rvert < \lvert\overline{D_{12,12}S_1}\rvert$, $x_{W_{4,12}} < x_{D_{12,12}}$, $r_u \leq \lvert\overline{OT_{1_A,11}}\rvert$	3.iii.b
$r_l \leq r_s$, $\lvert\overline{OD_{12,12}}\rvert < r_l$, $x_{W_{4,12}} < r_l \sin(\theta_s/2)$, $r_u \leq \lvert\overline{OT_{1_B,12}}\rvert$, $\lvert\overline{L_{1_B,1}S_1}\rvert < \lvert\overline{T_{1_A,12}S_1}\rvert$	4.i.a
$\lvert\overline{OD_{12,12}}\rvert < r_l$, $x_{W_{4,12}} < r_l \sin(\theta_s/2)$, $r_u \leq \lvert\overline{OT_{1_A,11}}\rvert$, $\lvert\overline{OT_{1_B,12}}\rvert < \lvert\overline{OT_{1_A,11}}\rvert$	4.i.b
$\lvert\overline{OD_{12,12}}\rvert < r_l$, $x_{W_{4,12}} < r_l \sin(\theta_s/2)$, $r_u < \lvert\overline{OW_{3,12}}\rvert$, $\lvert\overline{OT_{1_B,12}}\rvert < r_l$	4.ii
$r_l \leq r_s$, $\lvert\overline{D_{12,12}S_1}\rvert < \lvert\overline{L_{1_B,1}S_1}\rvert$, $x_{W_{4,12}} < x_{D_{12,12}}$, $\lvert\overline{OD_{12,12}}\rvert < \lvert\overline{OW_{3,12}}\rvert \leq r_u$	4.iii.a
$\lvert\overline{L_{1_A,1}S_1}\rvert < \lvert\overline{D_{12,12}S_1}\rvert$, $x_{W_{4,12}} < x_{D_{12,12}}$, $\lvert\overline{OD_{12,12}}\rvert < \lvert\overline{OW_{3,12}}\rvert \leq r_u$	4.iii.b
$r_l \leq r_s$, $\lvert\overline{OD_{12,12}}\rvert < r_l$, $x_{W_{4,12}} < r_l \sin(\theta_s/2)$, $\lvert\overline{OW_{3,12}}\rvert < r_u$, $r_l < \lvert\overline{OT_{1_B,12}}\rvert$, $\lvert\overline{OT_{1_A,11}}\rvert < \lvert\overline{OT_{1_B,12}}\rvert$, $\lvert\overline{L_{1_B,1}S_1}\rvert < \lvert\overline{T_{1_A,12}S_1}\rvert$	5.i.a
$\lvert\overline{OD_{12,12}}\rvert < r_l$, $x_{W_{4,12}} < r_l \sin(\theta_s/2)$, $\lvert\overline{OW_{3,12}}\rvert < r_u$, $r_l < \lvert\overline{OT_{1_A,11}}\rvert$, $\lvert\overline{OT_{1_B,12}}\rvert < \lvert\overline{OT_{1_A,11}}\rvert$	5.i.b
$r_l \leq r_s$, $\lvert\overline{D_{12,12}S_1}\rvert < \lvert\overline{L_{1_B,1}S_1}\rvert$, $x_{W_{4,12}} < x_{D_{12,12}}$, $r_u < \lvert\overline{OW_{3,12}}\rvert$, $\lvert\overline{OT_{1_B,12}}\rvert < r_u$	5.ii.a
$\lvert\overline{L_{1_A,1}S_1}\rvert < \lvert\overline{D_{12,12}S_1}\rvert$, $x_{W_{4,12}} < x_{D_{12,12}}$, $r_u < \lvert\overline{OW_{3,12}}\rvert$, $\lvert\overline{T_{1_A,11}S_1}\rvert < \lvert\overline{U_{1_A,1}S_1}\rvert$	5.ii.b
$r_l < \lvert\overline{OW_{4,12}}\rvert < \lvert\overline{OM_{12}}\rvert$, $\lvert\overline{OD_{12,12}}\rvert < \lvert\overline{OW_{4,12}}\rvert < \lvert\overline{OM_{12}}\rvert$, $r_u < \lvert\overline{OW_{3,12}}\rvert$, $r_l < \lvert\overline{OT_{1_A,12}}\rvert < r_u$, $r_l < \lvert\overline{OT_{1_B,12}}\rvert < r_u$	5.iii
$\lvert\overline{OD_{12,12}}\rvert < r_l$, $x_{W_{4,12}} < r_l \sin(\theta_s/2)$, $r_u < \lvert\overline{OW_{3,12}}\rvert$, $r_l < \lvert\overline{OT_{1_B,12}}\rvert < r_u$, $\lvert\overline{OT_{1_A,11}}\rvert < \lvert\overline{OT_{1_B,12}}\rvert$	6.i.a
$\lvert\overline{OD_{12,12}}\rvert < r_l$, $x_{W_{4,12}} < r_l \sin(\theta_s/2)$, $r_u < \lvert\overline{OW_{3,12}}\rvert$, $r_l < \lvert\overline{OT_{1_A,11}}\rvert < r_u$, $\lvert\overline{OT_{1_B,12}}\rvert < \lvert\overline{OT_{1_A,11}}\rvert$	6.i.b
$\lvert\overline{OD_{12,12}}\rvert < \lvert\overline{OW_{4,12}}\rvert < \lvert\overline{OM_{12}}\rvert$, $x_{W_{4,12}} < r_l \sin(\theta_s/2)$, $r_u < \lvert\overline{OW_{3,12}}\rvert$, $r_l < \lvert\overline{OT_{1_A,12}}\rvert < r_u$, $r_u < \lvert\overline{OT_{1_B,12}}\rvert$	6.ii
$r_l < \lvert\overline{OW_{4,12}}\rvert < \lvert\overline{OM_{12}}\rvert$, $\lvert\overline{OD_{12,12}}\rvert < \lvert\overline{OW_{4,12}}\rvert < \lvert\overline{OM_{12}}\rvert$, $\lvert\overline{OW_{3,12}}\rvert < r_u$, $\lvert\overline{OM_{12}}\rvert < \lvert\overline{OT_{1_B,12}}\rvert$	6.iii
$r_l < \lvert\overline{OW_{4,12}}\rvert < \lvert\overline{OM_{12}}\rvert$, $\lvert\overline{OD_{12,12}}\rvert < \lvert\overline{OW_{4,12}}\rvert < \lvert\overline{OM_{12}}\rvert$, $r_u < \lvert\overline{OW_{3,12}}\rvert$, $r_l < \lvert\overline{OT_{1_A,12}}\rvert < r_u$, $r_l < \lvert\overline{OT_{1_B,12}}\rvert \leq r_u$	7.i
$x_{W_{4,12}} < r_l \sin(\theta_s/2)$, $\lvert\overline{OD_{12,12}}\rvert < \lvert\overline{OW_{4,12}}\rvert < \lvert\overline{OM_{12}}\rvert$, $\lvert\overline{OW_{3,12}}\rvert < r_u$, $\lvert\overline{OM_{12}}\rvert < \lvert\overline{OT_{1_B,12}}\rvert$	7.ii
$x_{W_{4,12}} < r_l \sin(\theta_s/2)$, $\lvert\overline{OD_{12,12}}\rvert < \lvert\overline{OW_{4,12}}\rvert < \lvert\overline{OM_{12}}\rvert$, $r_u < \lvert\overline{OW_{3,12}}\rvert$, $r_l < \lvert\overline{OT_{1_A,12}}\rvert < r_u$, $r_l < \lvert\overline{OT_{1_B,12}}\rvert < r_u$	8

Table 3. Piecewise Formulation for 2-fold Coverage Area $\mathbf{A}'_{2\times,12}$

Shape Type	2-fold Coverage Area $\mathbf{A}'_{2\times,12}$
2	$2\mathbf{A}_{\Sigma}(R, \lvert\overline{W_{3,12}W_{4,12}}\rvert)$
3.i	$\mathbf{A}_{\Lambda_3}(r_l, R, \lvert\overline{A_{1,1}A_{2,2}}\rvert, \lvert\overline{A_{1,1}W_{3,12}}\rvert, \lvert\overline{A_{2,2}W_{3,12}}\rvert)$
3.ii	$\mathbf{A}_{\Lambda_4}(r_u, R, \lvert\overline{B_{1,1}B_{2,2}}\rvert, \lvert\overline{B_{1,1}W_{4,12}}\rvert, \lvert\overline{B_{2,2}W_{4,12}}\rvert)$
3.iii.a	$\mathbf{A}_{\Lambda_5}(r_u, \lvert\overline{U_{1_B,1}U_{2_B,2}}\rvert, \lvert\overline{U_{1_B,1}D_{12,12}}\rvert, \lvert\overline{U_{2_B,2}D_{12,12}}\rvert)$
3.iii.b	$\mathbf{A}_{\Lambda_5}(r_u, \lvert\overline{U_{2_A,2}U_{1_A,1}}\rvert, \lvert\overline{U_{2_A,2}D_{12,12}}\rvert, \lvert\overline{U_{1_A,1}D_{12,12}}\rvert)$
4.i.a	$\mathbf{A}_{\Pi_1}(r_u, r_l, U_{1_B,1}, U_{2_B,2}, L_{2_B,2}, L_{1_B,1})$
4.i.b	$\mathbf{A}_{\Pi_1}(r_u, r_l, U_{2_A,2}, U_{1_A,1}, L_{1_A,1}, L_{2_A,2})$
4.ii	$\mathbf{A}_{\Pi_2}(r_u, r_l, R, B_{2,2}, B_{1,1}, A_{1,1}, A_{2,2})$
4.iii.a	$\mathbf{A}_{\Pi_3}(R, R, W_{3,12}, T_{2_B,21}, D_{12,12}, T_{1_B,12})$
4.iii.b	$\mathbf{A}_{\Pi_3}(R, R, W_{3,12}, T_{1_A,11}, D_{12,12}, T_{2_A,22})$
5.i.a	$\mathbf{A}_{\Pi_1}(R, r_l, W_{3,12}, T_{2_B,21}, L_{2_B,2}, L_{1_B,1})+$ $\mathbf{A}_{\Lambda_5}(R, \lvert\overline{T_{1_B,12}W_{3,12}}\rvert, \lvert\overline{W_{3,12}L_{1_B,1}}\rvert, \lvert\overline{L_{1_B,1}T_{1_B,12}}\rvert)$
5.i.b	$\mathbf{A}_{\Pi_1}(R, r_l, W_{3,12}, T_{1_A,11}, L_{1_A,1}, L_{2_A,2})+$ $\mathbf{A}_{\Lambda_5}(R, \lvert\overline{T_{2_A,22}W_{3,12}}\rvert, \lvert\overline{W_{3,12}L_{2_A,2}}\rvert, \lvert\overline{L_{2_A,2}T_{2_A,22}}\rvert)$
5.ii.a	$\mathbf{A}_{\Pi_4}(r_u, R, R, B_{2,2}, B_{1,1}, T_{2_B,21}, T_{1_B,12})+$ $\mathbf{A}_{\triangle}(\lvert\overline{T_{2_B,21}D_{12,12}}\rvert, \lvert\overline{D_{12,12}T_{1_B,12}}\rvert, \lvert\overline{T_{1_B,12}T_{2_B,21}}\rvert)$
5.ii.b	$\mathbf{A}_{\Pi_4}(r_u, R, R, B_{2,2}, B_{1,1}, T_{1_A,11}, T_{2_A,22})+$ $\mathbf{A}_{\triangle}(\lvert\overline{T_{1_A,11}D_{12,12}}\rvert, \lvert\overline{D_{12,12}T_{2_A,22}}\rvert, \lvert\overline{T_{2_A,22}T_{1_A,11}}\rvert)$
5.iii	$\mathbf{A}_{\Pi_5}(r_u, U_{1_B,1}, U_{2_B,2}, T_{2_A,21}, T_{1_A,12})+$ $\mathbf{A}_{\Lambda_6}(R, R, \lvert\overline{T_{2_A,21}W_{4,12}}\rvert, \lvert\overline{W_{4,12}T_{1_A,12}}\rvert, \lvert\overline{T_{1_A,12}T_{2_A,21}}\rvert)$
6.i.a	$\mathbf{A}_{\Pi_1}(r_u, r_l, B_{2,2}, B_{1,1}, L_{2_B,2}, L_{1_B,1})+$ $\mathbf{A}_{\Lambda_5}(R, \lvert\overline{B_{1,1}T_{2_A,21}}\rvert, \lvert\overline{T_{2_A,21}L_{2_B,2}}\rvert, \lvert\overline{L_{2_B,2}B_{1,1}}\rvert)+$ $\mathbf{A}_{\Lambda_5}(R, \lvert\overline{T_{1_B,12}B_{2,2}}\rvert, \lvert\overline{B_{2,2}L_{1_B,1}}\rvert, \lvert\overline{L_{1_B,1}T_{1_B,12}}\rvert)$
6.i.b	$\mathbf{A}_{\Pi_1}(r_u, r_l, B_{2,2}, B_{1,1}, L_{1_A,1}, L_{2_A,2})+$ $\mathbf{A}_{\Lambda_5}(R, \lvert\overline{B_{1,1}T_{1_A,11}}\rvert, \lvert\overline{T_{1_A,11}L_{1_A,1}}\rvert, \lvert\overline{L_{1_A,1}B_{1,1}}\rvert)+$ $\mathbf{A}_{\Lambda_5}(R, \lvert\overline{T_{2_A,22}B_{2,2}}\rvert, \lvert\overline{B_{2,2}L_{2_A,2}}\rvert, \lvert\overline{L_{2_A,2}T_{2_A,22}}\rvert)$
6.ii	$\mathbf{A}_{\Pi_5}(r_u, U_{1_B,1}, U_{2_B,2}, T_{2_A,21}, T_{1_A,12}) + \mathbf{A}_{\Pi_6}(r_l, R, R, A_{1,1}, A_{2,2}, T_{1_A,12}, T_{2_A,21})$
6.iii	$\mathbf{A}_{\square}(T_{2_B,21}, T_{2_A,21}, T_{1_A,12}, T_{1_B,12})+$ $\mathbf{A}_{\Lambda_6}(R, R, \lvert\overline{T_{1_B,12}W_{3,12}}\rvert, \lvert\overline{W_{3,12}T_{2_B,21}}\rvert, \lvert\overline{T_{2_B,21}T_{1_B,12}}\rvert)+$ $\mathbf{A}_{\Lambda_6}(R, R, \lvert\overline{T_{2_A,21}W_{4,12}}\rvert, \lvert\overline{W_{4,12}T_{1_A,12}}\rvert, \lvert\overline{T_{1_A,12}T_{2_A,21}}\rvert)$
7.i	$\mathbf{A}_{\Pi_4}(r_u, R, R, B_{2,2}, B_{1,1}, T_{2_B,21}, T_{1_B,12}) + \mathbf{A}_{\square}(T_{2_B,21}, T_{2_A,21}, T_{1_A,12}, T_{1_B,12})+$ $\mathbf{A}_{\Lambda_6}(R, R, \lvert\overline{T_{2_A,21}W_{4,12}}\rvert, \lvert\overline{W_{4,12}T_{1_A,12}}\rvert, \lvert\overline{T_{1_A,12}T_{2_A,21}}\rvert)$
7.ii	$\mathbf{A}_{\Lambda_6}(R, R, \lvert\overline{T_{1_B,12}W_{3,12}}\rvert, \lvert\overline{W_{3,12}T_{2_B,21}}\rvert, \lvert\overline{T_{2_B,21}T_{1_B,12}}\rvert)+$ $\mathbf{A}_{\square}(T_{2_B,21}, T_{2_A,21}, T_{1_A,12}, T_{1_B,12}) + \mathbf{A}_{\Pi_6}(r_l, R, R, A_{1,1}, A_{2,2}, T_{1_A,12}, T_{2_A,21})$
8	$\mathbf{A}_{\Pi_4}(r_u, R, R, B_{2,2}, B_{1,1}, T_{2_B,21}, T_{1_B,12}) + \mathbf{A}_{\square}(T_{2_B,21}, T_{2_A,21}, T_{1_A,12}, T_{1_B,12})+$ $\mathbf{A}_{\Pi_6}(r_l, R, R, A_{1,1}, A_{2,2}, T_{1_A,12}, T_{2_A,21})$

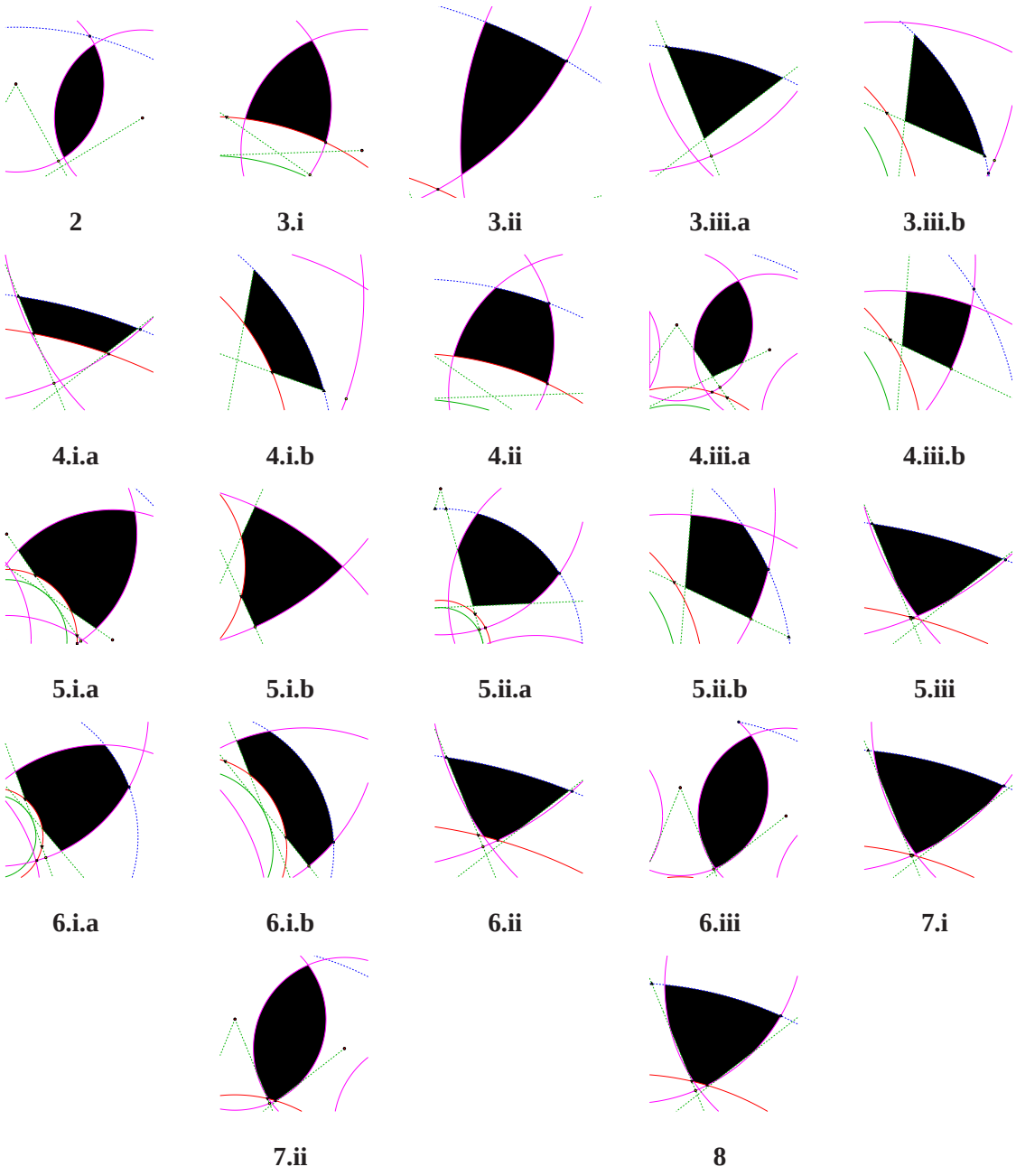

Figure 4. Taxonomy of Overlap Areas $A'_{2\times,12}$ (shaded black)

PARTIAL CONDITIONS ON THE EXISTENCE OF 2-FOLD COVERAGE

This section aims to determine explicitly the coverage multiplicities present for a given constellation at an instant in time using arguments based on shell intersections. Due to the complexity of this endeavor, exhaustive conditions are outside the scope of this paper. However, partial conditions are provided to illustrate a basic approach that could be used to derive the remaining conditions.

In a sense, coverage multiplicities are created and destroyed systematically. There are several

ways in which this can occur, but to adhere to previously made assumptions, the conditions presented here focus on one of these ways in which coverage multiplicities are manifested. Necessary conditions for the existence of 2-fold coverage (or less) for adjacent satellites are

$$\begin{aligned} m_{1,1} &\neq m_{2,2} \\ d_{12} &< 2R \\ \|\overline{OD_{12,12}}\| &< r_u \end{aligned} \tag{43}$$

Sufficient conditions are

$$|\overline{HS_2}| < R \tag{44}$$

where H is an auxiliary point defined in Table 4, covering all possible parameter configurations. A detailed derivation of these results is omitted, but a brief explanation follows. Notice in Figure 3 that a line drawn from the origin to $W_{3,12}$ bisects the region $C'_{2\times,12}$. By definition, 2-fold coverage is created at a point H on this bisector and within the region of interest. In the absence of altitude shells, 2-fold coverage would be created at the midpoint $H = M_{12}$, but when altitude shells are taken into account, the location of H depends on the satellite altitude and other factors. Also, note in Table 4 the modified notation $(D_{12,12})_y = y_{D_{12,12}}$. To ensure that no coverage multiplicities greater than two exist, a condition is imposed stating that triplets of adjacent satellites cannot intersect:

$$d_{2n} \geq 2R \tag{45}$$

which precludes the existence of coverage multiplicities $p \geq 3$.

Table 4. Sufficient Condition Flow Chart for Existence of Coverage Multiplicity $p = 2$

	Conditions		H
$r_t \leq r_s \leq r_l$	$\|\overline{OD_{12,12}}\| \leq r_l$		$(r_l \sin\frac{\pi}{n}, r_l \cos\frac{\pi}{n})$
	$r_l < \|\overline{OD_{12,12}}\|$		$D_{12,12}$
$r_l \leq r_s \leq r_u$	$(M_{12})_y \leq r_l \cos\frac{\pi}{n}$	$\|\overline{OD_{12,12}}\| \leq r_l$	$(r_l \sin\frac{\pi}{n}, r_l \cos\frac{\pi}{n})$
		$r_l < \|\overline{OD_{12,12}}\|$	$D_{12,12}$
	$r_l \cos\frac{\pi}{n} < (M_{12})_y$	$(D_{12,12})_y \leq (M_{12})_y$	M_{12}
		$(M_{12})_y < (D_{12,12})_y$	$D_{12,12}$
$r_u \leq r_s \leq r_{s3}$	$(M_{12})_y \leq r_l \cos\frac{\pi}{n}$	$\|\overline{OD_{12,12}}\| \leq r_l$	$(r_l \sin\frac{\pi}{n}, r_l \cos\frac{\pi}{n})$
		$r_l < \|\overline{OD_{12,12}}\|$	$D_{12,12}$
	$r_l \cos\frac{\pi}{n} < (M_{12})_y < r_u \cos\frac{\pi}{n}$	$(D_{12,12})_y \leq (M_{12})_y$	M_{12}
		$(M_{12})_y < (D_{12,12})_y$	$D_{12,12}$
	$r_u \cos\frac{\pi}{n} \leq (M_{12})_y$		$(r_u \sin\frac{\pi}{n}, r_u \cos\frac{\pi}{n})$

PARAMETER SPACE AND VALIDATION OF NUMERICAL METHODS

With the preceding analysis complete, initial exploration of the parameter space can be performed. Figures 5-7 show three possible types of behavior for how the total coverage area varies with satellite altitude, h_s, when all other parameters are held fixed. Figure 5 shows a case where there is a clear optimal satellite altitude corresponding to a maximum coverage area provided by the constellation. Under other conditions, as shown in Figure 6, saturation can occur at low satellite altitudes; these are regimes in which varying h_s offers no coverage benefit. Another interesting artifact of total coverage area is observed in Figure 7, where a sharp corner is apparent near $h_s \approx 10,820$ km. The explanation for this is that the overlap area shape $C'_{2\times,12}$ changes type rapidly over a small range — approximately 70 km — of satellite altitude.

Another purpose of this analysis is to provide an analytical means of validating the numerical process proposed by Takano.[5,6] The numerical algorithm employed by Takano is generally applicable to the time-varying and the time-invariant case, with generalized sensor profiles. However, since closed form solutions are not available in the generalized case, an intermediate step is to validate a set of simplified cases, such as those discussed here. For example, the simulation results presented in Figures 5-7 do not encompass all possible scenarios, but do validate a subset of satellite configurations in a single circular orbit against the numerical model derived by Takano.[5,6]

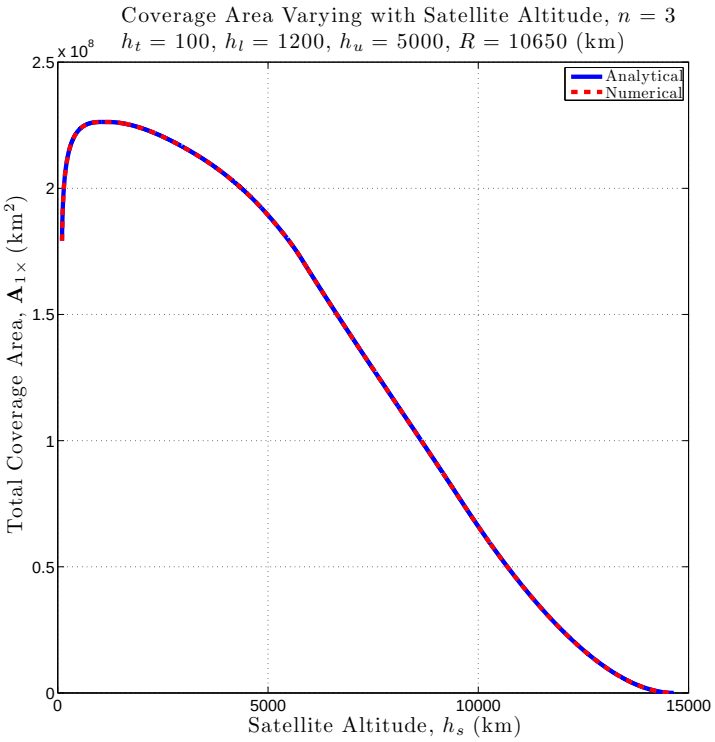

Figure 5. Total coverage area vs. satellite altitude (Example 1) is a continuous smooth curve: Optimal altitude corresponds to maximum coverage area

Figures 5-7 compare analytical and numerical results for continuous coverage area by fixing all parameters and then increasing the satellite altitude. Further notice that the fixed parameter

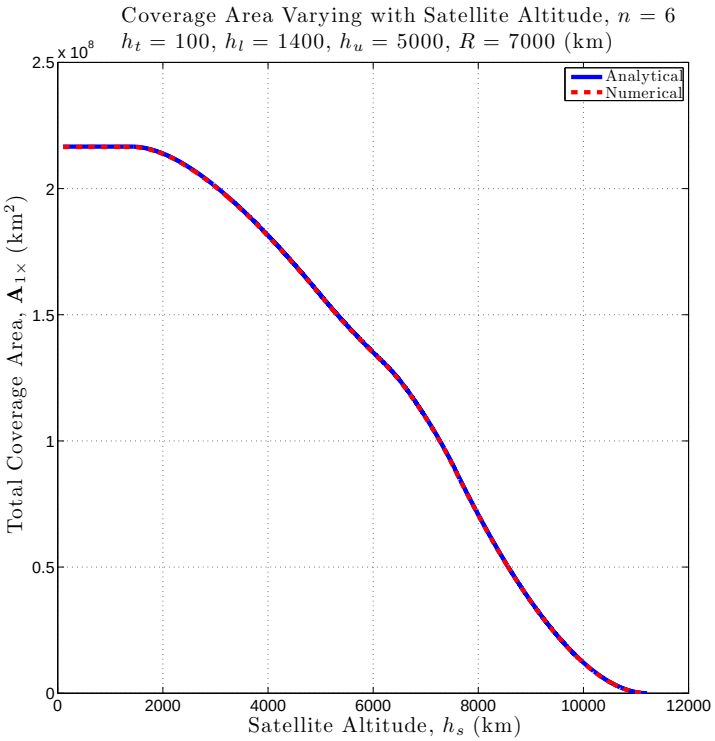

Figure 6. Total coverage area vs. satellite altitude (Example 2) is a continuous smooth curve: Maximum coverage area saturation observed at low altitudes

values are different in each simulation. The present study seeks to provide complete validation of the numerical process under the stated simplified set of assumptions, including the constellation coverage area calculation and the 2-fold coverage constraint. The numerical approach[5,6] considers a cost index determined numerically through the synthesis of computer graphics methods. The process employed here, in contrast, provides validation with an analytically determined cost index.

CONCLUSION

The problem of constellation design for space-based space situational awareness applications is considered from an analytical perspective. First, geometrical arguments are employed to establish an analytical formulation for coverage area provided by a planar constellation of equally spaced satellites with omnidirectional sensors. This leads to a piecewise differentiable exact representation for the coverage area provided by the constellation above the horizon of each satellite. Analytical conditions for coverage multiplicity are also established. The results of this investigation are successfully validated against a generalized numerical algorithm developed under a parallel study.

ACKNOWLEDGMENT

This research was carried out at The University of Texas at Austin and was funded by the Air Force Office of Scientific Research through the Air Force Young Investigator Award, contract # FA9550-09-1-0227. Any opinions, findings, and conclusions or recommendations expressed in this

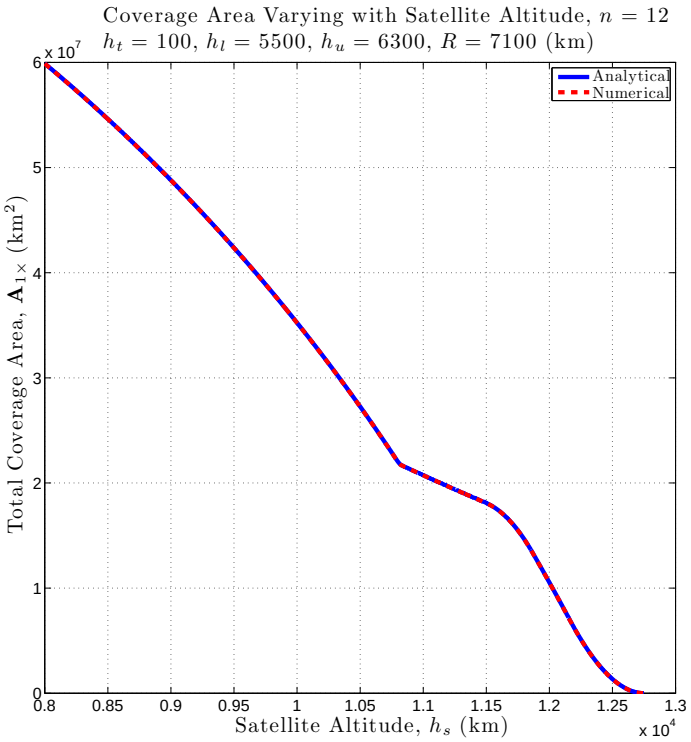

Figure 7. Total coverage area vs. satellite altitude (Example 3) is a continuous non-smooth curve: Global maximum exists only at the start of the altitude range considered

material are those of the authors and do not necessarily reflect the views of the funding agency.

REFERENCES

[1] B. G. Marchand and C. J. Kobel, "Above the Horizon Satellite Coverage with Dual-Altitude Band Constraints," *Journal of Spacecraft and Rockets*, Vol. 46, No. 4, 2009, pp. 845–857.

[2] L. Rider, "Design of Low to Medium Altitude Surveillance Systems Providing Continuous Multiple Above-the-Horizon Viewing," *Optical Engineering*, Vol. 28, Jan. 1989, pp. 25–29.

[3] R. D. Lüders, "Satellite Networks for Continuous Zonal Coverage," *American Rocket Society Journal*, Vol. 31, Feb. 1961, pp. 179–184.

[4] W. S. Adams and L. Rider, "Circular Polar Constellations Providing Continuous Single or Multiple Coverage Above a Specified Latitude," *Journal of the Astronautical Sciences*, Vol. 35, April-June 1987, pp. 155–192.

[5] A. Takano, "Numerical Analysis and Design of Satellite Constellations for Above the Horizon Coverage," Master's thesis, The University of Texas at Austin, December 2010.

[6] A. Takano, "Optimal Constellation Design for Space Based Situational Awareness Applications: A Numerical Approach," *Proceedings of the AAS/AIAA Astrodynamics Conference*, 2011.

[7] M. P. Fewell, "Area of Common Overlap of Three Circles," tech. rep., Maritime Operations Div., Defence Science and Technology Organisation, Oct. 2006. TN DSTO-TN-0722.

[8] E. W. Weisstein, "Bretschneider's Formula," From MathWorld–A Wolfram Web Resource. http://mathworld.wolfram.com/BretschneidersFormula.html.